JACS
JOURNAL OF THE AMERICAN CHEMICAL SOCIETY
Article
pubs.acs.org/JACS

Solid-State NMR Investigation of the Conformation, Proton Conduction, and Hydration of the Influenza B Virus M2 Transmembrane Proton Channel

Jonathan K. Williams,[†] Daniel Tietze,[†,§] Myungwoon Lee,[†] Jun Wang,[‡] and Mei Hong*[,†]

[†]Department of Chemistry, Massachusetts Institute of Technology, Cambridge, Massachusetts 02139, United States
[‡]Department of Pharmacology and Toxicology, The University of Arizona, Tucson, Arizona 85721, United States

ABSTRACT: Together with the influenza A virus, influenza B virus causes seasonal flu epidemics. The M2 protein of influenza B (BM2) forms a tetrameric proton-conducting channel that is important for the virus lifecycle. BM2 shares little sequence homology with AM2, except for a conserved HxxxW motif in the transmembrane (TM) domain. Unlike AM2, no antiviral drugs have been developed to block the BM2 channel. To elucidate the proton-conduction mechanism of BM2 and to facilitate the development of BM2 inhibitors, we have employed solid-state NMR spectroscopy to investigate the conformation, dynamics, and hydration of the BM2 TM domain in lipid bilayers. BM2 adopts an α-helical conformation in lipid membranes. At physiological temperature and low pH, the proton-selective residue, His19, shows relatively narrow ^{15}N chemical exchange peaks for the imidazole nitrogens, indicating fast proton shuttling that interconverts cationic and neutral histidines. Importantly, pH-dependent ^{15}N chemical shifts indicate that His19 retains the neutral population to much lower pH than His37 in AM2, indicating larger acid-dissociation constants or lower pK_a's. We attribute these dynamical and equilibrium differences to the presence of a second titratable histidine, His27, which may increase the proton-dissociation rate of His19. Two-dimensional ^{1}H−^{13}C correlation spectra probing water ^{1}H polarization transfer to the peptide indicates that the BM2 channel becomes much more hydrated at low pH than at high pH, particularly at Ser12, indicating that the pore-facing serine residues in BM2 mediate proton relay to the proton-selective histidine.

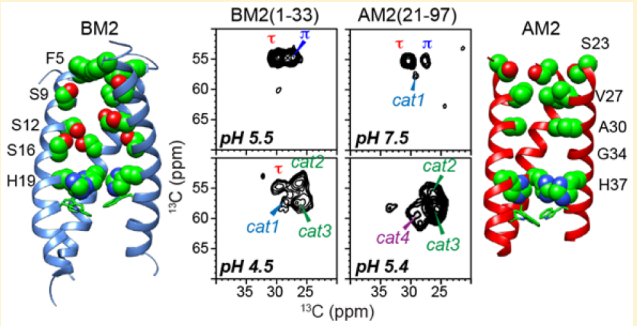

INTRODUCTION

While influenza viruses are best known for causing devastating flu pandemics in history, they exert just as much economic and social burden by causing seasonal flu epidemics. Two types of influenza viruses, A and B, are responsible for the seasonal flu. On average influenza A infections are more common in the seasonal flu,[1] but the influenza B virus becomes dominant in the spring months, and in some seasons can account for up to 50% of infections (data available from CDC FluView, www.cdc.gov/flu/weekly/).[2]

The currently approved adamantane class of antiviral drugs works only against the influenza A virus by binding to its M2 protein (AM2) and blocking the conduction of protons into the virus, a process that is important for the virus lifecycle.[3−7] However, these drugs have no effect against the influenza B M2 protein (BM2), which also has proton-channel activity.[8] The lack of inhibition is not surprising: BM2 and AM2 share little sequence homology, with only a HxxxW motif conserved in their respective TM domains (Figure 1a).[9] The histidine is responsible for the acid activation and proton selectivity of the channel, whereas the tryptophan is responsible for channel gating.[8,10] Sequence alignment of the two TM domains shows that the BM2 channel pore is significantly more polar than the AM2 channel, with multiple Ser residues lining the pore, suggesting the reason for the inability of the hydrophobic adamantane to inhibit BM2.[11]

A high-resolution solution NMR structure of the BM2 TM domain has been determined using BM2(1−33) bound to DHPC micelles.[12] The result shows a coiled-coil tetramer with three Ser residues (S9, S12, S16) lining the pore and a bulky Phe residue (F5) lying at the N-terminal entrance. The structure of the cytoplasmic domain was also determined in the same study using a BM2(26−109) construct. Liposome assays indicate that BM2(1−33) exhibits rimantadine-insensitive proton conductance, and in *Escherichia coli* lipid extracts, the single-channel conductance of BM2(1−33) is 2-fold higher than the conductance of AM2(18−60).[12] Since AM2(18−60) has the same specific activity as full-length AM2,[13] and whole-cell voltage-clamp assays of full-length AM2 and BM2 indicate similar inward proton currents,[8] these data together indicate that BM2(1−33) encompasses the full channel activity of the intact protein. Similar to AM2, BM2's channel activity is important for virus uncoating[8,14] and for preventing hemagglutinin from prematurely adopting a low-pH conformation during transport to the cell surface.[8,15,16] The cytoplasmic domain of BM2 carries out the separate function of incorporation of M1 and viral ribonucleoprotein complexes at the virion budding site during virus assembly.[17,18]

Received: March 26, 2016
Published: June 10, 2016

DOI: 10.1021/jacs.6b03142
J. Am. Chem. Soc. 2016, 138, 8143−8155

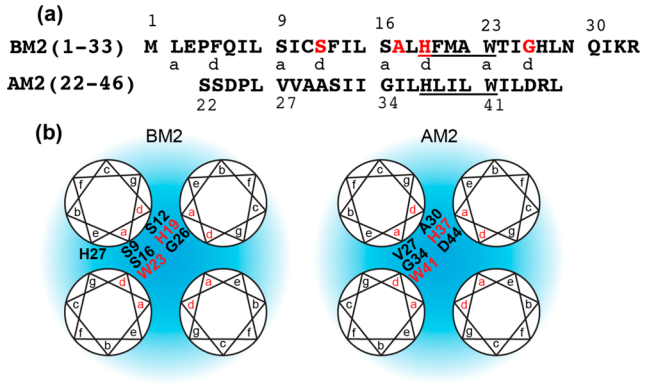

Figure 1. Comparison of the amino acid sequences (a) of the BM2 and AM2 transmembrane domains. Lowercase letters indicate heptad repeat, with a and d indicating pore-facing positions. The conserved HxxxW motif is underlined, and the ^{13}C,^{15}N-labeled residues are shown in red. (b) Four-helix bundle organization of the BM2 and AM2 transmembrane domains, with the pore-facing a and d residues indicated.

While AM2 and BM2 channels are functional analogues, various differences exist in their pH- and voltage-dependent proton conduction. The BM2 TM domain contains a second histidine (H27), C-terminal to the gating Trp23, whose mutation to Ala reduces the inward H^+ current by ~26%.[12] Whole-cell electrophysiological assays showed that BM2 has significant *outward* current under positive voltages, when the external pH (pH_{out}) is high and the internal pH (pH_{in}) is low, conditions under which AM2 shows negligible outward current.[8] To understand the basis for these functional differences, and to facilitate the design of antiviral drugs against influenza B infection, it is important to determine the structure of the BM2 TM domain in lipid bilayers and to investigate the mechanisms of action of the functional residues, His19 and Trp23.

A large amount of structural and dynamical information about the HxxxW motif has been obtained on the AM2 protein. The His37 residue in AM2 is now known to shuttle protons into the virion by proton exchange with water. ^{15}N chemical exchange peaks have been observed in both TM peptide and cytoplasmic-containing constructs of AM2 and in the S31N mutant of AM2.[19−22] The line widths of the exchange peaks differ, indicating that proton-transfer rates are sensitive to protein structural differences and electrostatic effects. This proton shuttling involves ring reorientations[23] and $\tau-\pi$ tautomerization.[22] Measured imidazole ^1H chemical shifts at low and high temperatures suggest hydrogen bonding between histidine and water;[7] in addition, His-His hydrogen bonding has also been proposed.[21,24] His37-Trp41 cation$-\pi$ interaction at low pH has been suggested by $^{13}C-^{19}F$[25] and $^{13}C-^{15}N$[26] distance experiments and UV resonance Raman experiments,[27] and has been proposed to regulate proton release from His to the C-terminal water molecules,[28,29] in agreement with the gating function of Trp.[10] Computed free-energy profiles of proton transport and 2D IR data indicate that proton conduction at low pH is facilitated by an expanded channel width and increased hydration and solvent dynamics.[30,31] The relation between channel hydration and His-mediated proton shuttling is of special interest, because the BM2 TM domain has a more polar pore-lining surface than AM2, suggesting that the histidine-mediated proton-transfer dynamics might differ from that of AM2.

Solid-state NMR spectroscopy is a powerful and versatile tool for studying the structure and dynamics of membrane proteins in lipid bilayers. Increasing evidence from studies of many membrane peptides and proteins indicates that the structures of small oligomeric membrane proteins are more susceptible to changes by the membrane environment compared to large membrane protein complexes and machineries,[32−37] and some of these structural changes are functionally relevant. Solid-state NMR based structural and dynamical studies of membrane proteins in phospholipid bilayers instead of detergents are therefore essential for obtaining biologically authentic mechanistic information. In this study, we investigate the backbone conformation of BM2(1−33) using chemical shifts of site-specifically labeled peptides, and then focus on the structures and dynamics of the proton-selective His19. We also investigate channel hydration using water−protein $^1H-^{13}C$ 2D correlation experiments. We show that in cholesterol-containing eukaryotic-mimetic membranes, BM2(1−33) is stably α-helical at high and low pH, and in two different membranes examined, and His19 exhibits a number of cationic and tautomeric states that in totality resemble those seen for His37 in AM2 but that have a shifted pH dependence. ^{15}N NMR spectra of His19 yielded four pK_a's, which are about one pH unit lower than the pK_a's of His37 in AM2. The BM2 channel hydration is both pH- and membrane-dependent: negatively charged membranes increased the pore hydration compared to neutral membranes, and the pH dependence of BM2 hydration is larger than that of AM2. These results suggest the structural reasons for some of the functional differences between these two viral proton channels, and how the amino acid sequence affects the histidine-mediated proton conduction.

MATERIALS AND METHODS

Synthesis of Isotopically Labeled BM2(1−33). A peptide corresponding to residues 1−33 (MLEPFQILS ICSFILSALH FMAWTIGHLN QIKR) of the B/Maryland/1/2001 strain of influenza virus was synthesized using Fmoc solid-phase peptide synthesis protocols as described previously.[22,38] Briefly, ChemMatrix Rink Amide resin was used for the peptide synthesis. For the coupling step, 5 equiv of amino acid, 5 equiv of HCTU, and 10 equiv of diisopropylamine were used, and the reaction was carried out in DMF for 5 min at 75 °C. For the Fmoc deprotection step, 5% piperazine in DMF plus 0.1 M HOBt were used, and the reaction was similarly carried out in DMF for 5 min at 75 °C. Final peptide cleavage from the resin was carried out in a cocktail that consists of 95% trifluoroacetic acid, 2.5% triisopropylsilane, and 2.5% H_2O for 2.5 h at room temperature. Cleaved peptide was precipitated in cold ether and purified by preparative HPLC (Vydac C4 Column). Uniformly ^{13}C,^{15}N-labeled amino acids (Sigma-Aldrich and Cambridge Isotope Laboratories) were introduced at positions S12, A17, His19, and G26.

Membrane Sample Preparation. The BM2(1−33) peptide was reconstituted into two lipid membranes, POPC:POPG:-cholesterol (PC/PG/Chol) at molar ratios of 60%:20%:20%, and POPC:POPE:sphingomyelin:cholesterol (VM+) at equimolar concentrations.[38] Both lipid mixtures mimic eukaryotic membranes by including cholesterol, but the former contains the anionic lipid POPG, since this mixture is commonly used in M2 proton conductance assays[12] and membrane scission assays.[39] Anionic lipids are also present in the plasma membrane and the virus lipid envelope at ~15 mol %, but usually in the form of phosphatidylserine instead of phosphatidylglycerol.[40] The neutral VM+ lipid mixture allows us to compare the structure of BM2 with that of AM2 in the same membrane.[38] The lipids were mixed together in chloroform, and then the solvent was

DOI: 10.1021/jacs.6b03142
J. Am. Chem. Soc. 2016, 138, 8143−8155

removed by nitrogen gas. The peptide was dissolved in 1 mL of 1,1,1,3,3,3-hexafluoro-2-propanol (HFIP) or 2,2,2-trifluoroethanol (TFE), and then mixed with the lipids. The bulk solvent was removed again by nitrogen gas, and then the powder was placed under vacuum at room temperature overnight followed by lyophilization for 2−3 h to fully remove fluorinated solvents. The resulting lipid−peptide mixture was suspended in buffer, vortexed, and freeze−thawed 8−10 times to create uniform vesicles. The proteoliposome solution was spun at 50 000 rpm at 4 °C for 4 h to obtain homogeneous membrane pellets. The pellets were allowed to dry slowly in a desiccator to 40−50% hydration by mass, and then transferred into 4 mm or 3.2 mm magic-angle-spinning (MAS) rotors for solid-state NMR experiments.

Seven BM2 samples were prepared at different pH in the two membranes. For the PC/PG/Chol membrane, three samples were prepared at pH 7.5 (10 mM Tris, 1 mM EDTA, 0.1 mM NaN_3), pH 5.5 and pH 4.5 (10 mM citric acid/citrate, 1 mM EDTA, 0.1 mM NaN_3) and the peptide:lipid molar ratio was 1:15. For the VM+ membrane, four samples were prepared at pH 6.5 (20 mM Bis-Tris, 2 mM EDTA, 0.2 mM NaN_3), pH 5.5 (10 mM citric acid/citrate, 1 mM EDTA, 0.1 mM NaN_3), pH 4.5 (10 mM citric acid/citrate, 1 mM EDTA, 0.1 mM NaN_3), and pH 4.0 (20 mM citric acid/citrate, 2 mM EDTA, 0.2 mM NaN_3). The peptide:lipid molar ratio was 1:13.3. The pH of the membrane samples was measured at two time points during sample preparation: after freeze−thawing to create homogeneous vesicle solutions, and after ultracentrifugation, where the supernatant pH was measured. The measured pH was within 0.1 pH units of the desired value.

Membrane Samples for Dynamic Nuclear Polarization (DNP) Experiments. BM2(1−33) was reconstituted into a deuterated lipid mixture denoted d_{31}-VM+′, which contains d_{31}-POPC, d_{31}-POPE, and cholesterol at a molar ratio of 40%:40%:20%.[41] The partially deuterated phospholipids were used to increase the efficiency of polarization transfer from the radical to the peptide. About 1 mg of BM2 was dissolved in TFE, and then mixed with the d_{31}-VM+′ lipid mixture in chloroform at a peptide/lipid molar ratio of 1:22.5. The organic solvents were removed under nitrogen gas, and then the mixture was lyophilized overnight. The peptide−lipid mixture was suspended in a 10 mM pH 5.5 citrate buffer and centrifuged at 40 000 rpm at 4 °C overnight to obtain a homogeneous pellet, which was equilibrated to a hydration level of ∼40 wt %. A small amount of a stock DNP solution, d_8-glycerol:D_2O:H_2O (60:30:10 by volume), containing 10 mM of the biradical AMUPol was titrated into the membrane pellet.[41] The pellet was vortexed to distribute the radical uniformly, and D_2O was added to reach a D_2O:H_2O volume ratio of 3:1. The sample was then allowed to equilibrate again to ∼40% hydration, and then packed into a 3.2 mm sapphire rotor and sealed with a silica plug for DNP experiments at 117 K.

Solid-State NMR Experiments. Solid-state NMR experiments were carried out on Bruker 400 MHz (9.4 T) and 800 MHz (18.8 T) NMR spectrometers using 4 mm or 3.2 mm $^1H/^{13}C/^{15}N$ MAS probes. Typical radiofrequency (rf) field strengths were 71−83 kHz for ^1H, 62.5−71 kHz for ^{13}C, and 45−50 kHz for ^{15}N. Chemical shifts were referenced to the CH_2 signal of adamantane at 38.48 ppm on the tetramethylsilane (TMS) scale for ^{13}C, the amide signal of N-acetylvaline at 122.0 ppm on the liquid ammonia scale for ^{15}N, and the Hγ signal of the lipid phosphocholine headgroup at 3.26 ppm on the TMS scale for ^1H.

One-dimensional ^{13}C and ^{15}N cross-polarization (CP) MAS spectra were measured at 313−243 K. To extract His19 pK_a's, we measured ^{15}N CP-MAS spectra of the four VM+ bound BM2 samples at 243 K on the 400 MHz spectrometer. About 100 000 scans were averaged for each sample to obtain sufficient sensitivity. The $^1H-^{15}N$ CP contact time was 3 ms, and the ^1H and ^{15}N spin-lock matching condition was optimized by maximizing the 250-ppm unprotonated ^{15}N peak in a pH 8.5 histidine model compound. The ratio of the integrated intensities of the unprotonated to the protonated ^{15}N peaks in amino acid histidine ranged from 1.35 to 1.45, reflecting incomplete polarization transfer to the unprotonated nitrogen. This factor is taken into account in extracting the ratio of neutral to cationic His19 in BM2.

Two-dimensional (2D) $^{13}C-^{13}C$ correlation spectra were measured using a proton-driven spin-diffusion experiment with dipolar-assisted rotational resonance (DARR) mixing.[42] The 400 MHz data were acquired at 243 K with a spin-diffusion mixing time of 50 ms, while the 800 MHz data were obtained at 263 K using a mixing time of 100 ms. Two-dimensional $^{15}N-^{13}C$ heteronuclear correlation (HETCOR) spectra were measured at 263 K using a REDOR based pulse sequence[43] with dipolar mixing times of 0.5−0.6 ms.

A 2D $^1H-^{13}C$ HETCOR experiment with spin diffusion[44−46] was used to measure the hydration of BM2 residues. A ^1H T_2 filter of 1−6 ms was used before spin diffusion to suppress the peptide ^1H magnetization while retaining most of the water and lipid ^1H magnetization. Two ^1H spin-diffusion mixing times were measured for each sample, a short mixing time of 4 ms and a long mixing time, which was 50 ms for the pH 7.5 PC/PG/Chol sample and 100 ms for the pH 5.5 PC/PG/Chol sample and the VM+ samples. Due to the different phase transition temperatures of the two membranes, the PC/PG/Chol samples were measured at 263 K while the VM+ samples were measured at 293 K. Water ^1H T_1 relaxation times were measured using an inversion recovery sequence and range from ∼230 to ∼850 ms. The pH 7.5 PC/PG/Chol membrane showed the shortest water ^1H T_1 relaxation time (∼230 ms); thus, we chose a long mixing time of 50 ms instead of 100 ms for this sample to obtain sufficient sensitivity. On the basis of our studies of water interactions with a number of membrane peptides and proteins such as AM2,[46,47] antimicrobial peptides,[34,48] and bacterial toxins,[45,49] the 50 ms mixing is sufficient to equilibrate the water polarization with BM2. Water ^1H cross-peak intensities with peptide ^{13}C signals were extracted from the cross section of each 2D spectrum, and the intensity ratios between the short and long mixing-time spectra were corrected for ^1H T_1 relaxation according to $S/S_0 = S(4\text{ ms})e^{4\text{ms}/T_1}/S(100\text{ ms})e^{100\text{ms}/T_1}$ or $S/S_0 = S(4\text{ ms})e^{4\text{ms}/T_1}/S(50\text{ ms})e^{50\text{ms}/T_1}$ to give the initial spin-diffusion buildup intensity from water to the protein residue. Error bars for S/S_0 values were propagated from the signal-to-noise ratios of the peaks.

DNP Experiment Conditions. DNP spectra were measured on the pH 5.5 BM2 sample bound to the d_{31}-VM+′ membrane on a 400 MHz/263 GHz DNP spectrometer at Bruker Biospin (Billerica, MA). The sample temperatures were ∼108 K with the microwave (MW) off and ∼117 K with the MW on at 130 mA. Double-quantum-filtered (DQF) 1D ^{13}C spectra were measured using 2.2 ms of SPC5 $^{13}C-^{13}C$ dipolar recoupling.[50] One-dimensional and 2D $^{15}N-^{13}C$ dipolar filtered spectra were measured using a double CP pulse sequence with a $^1H-^{15}N$ CP contact time of 1.25 ms and a $^{15}N-^{13}C$ CP contact time of 9.0 ms.

DOI: 10.1021/jacs.6b03142
J. Am. Chem. Soc. 2016, 138, 8143−8155

Extraction of His19 pK_a's. His19 acid-dissociation constants (K_a's) were extracted from the ^{15}N CP-MAS spectra based on the fact that the neutral-to-cationic hisitidine concentration ratios are reflected by the relative intensities of the protonated NH peaks and the unprotonated nitrogen peak according to $[\text{His}]/[\text{HisH}^+] = 2[(I_{NH}/I_N)/\kappa - 1]^{-1}$. ^{15}N peak intensities were integrated from 258 to 240 ppm for the unprotonated imidazole nitrogen, which results exclusively from neutral histidine, and 200−150 ppm for the protonated nitrogen, which results from both neutral and cationic histidines. The κ in the equation is a correction factor for the reduced efficiency of ^{1}H−^{15}N CP for the unprotonated nitrogen compared to protonated nitrogen. The κ value is measured from the optimized CP spectrum of pH 8.5 amino acid histidine.[51] The model-compound spectrum was measured with the same CP contact time, ^{1}H and ^{15}N radiofrequency matching conditions, and MAS frequency as for the BM2 samples. For these ^{15}N CP experiments, the samples were spun at 7 kHz, and a CP contact time of 3 ms was used. Uncertainties in the neutral-to-cationic histidine concentration ratios were propagated from the signal-to-noise ratios of the spectra.

The neutral-to-cationic histidine concentration ratios at different pH were fit using the equation[19,24]

$$\frac{[\text{His}]}{[\text{HisH}^+]} = \frac{1\cdot\frac{K_{a1}}{10^{-\text{pH}}} + 2\cdot\frac{K_{a1}\cdot K_{a2}}{10^{-2\text{pH}}} + 3\cdot\frac{K_{a1}\cdot K_{a2}\cdot K_{a3}}{10^{-3\text{pH}}} + 4\cdot\frac{K_{a1}\cdot K_{a2}\cdot K_{a3}\cdot K_{a4}}{10^{-4\text{pH}}}}{4 + 3\cdot\frac{K_{a1}}{10^{-\text{pH}}} + 2\cdot\frac{K_{a1}\cdot K_{a2}}{10^{-2\text{pH}}} + 1\cdot\frac{K_{a1}\cdot K_{a2}\cdot K_{a3}}{10^{-3\text{pH}}}} \quad (1)$$

in MATLAB's Curve Fitting Toolbox. Among the four pK_a's, pK_{a4} has the highest value and is for the first protonation event, while pK_{a1} corresponds to the last protonation event and has the lowest value. Uncertainties in the determined pK_a's were estimated from the uncertainty ranges of the histidine concentration ratios.

RESULTS

Backbone Conformation and Dynamics of BM2(1−33) in Lipid Membranes. We measured 1D and 2D ^{13}C spectra as a function of pH, membrane composition, and temperature (Figures 2 and 3) to determine the global conformation and dynamics of BM2(1−33). At low temperature (243 K), the labeled residues exhibit strong signals at α-helical chemical shifts in both PC/PG/Chol and VM+ membranes. The S12 Cα and Cβ cross peaks are close to the diagonal, characteristic of the α-helical conformation. Distinct α-helical Cα and Cβ chemical shifts are also observed for A17 and G26. Interestingly, for S12, A17, and G26, Cα and CO chemical shifts decrease at low pH compared to high pH (Table 1), suggesting that the local conformations at these residues become less ideally α-helical at acidic pH. The line widths also increase at low pH, indicative of larger conformational heterogeneity in the open state. Increasing the temperature to 303 K weakened most of the intensities of the PC/PG/Chol bound peptides while retaining the intensities of VM+ bound peptides (Figure 2a,b). This indicates that BM2(1−33) undergoes intermediate-time scale motion[52] in PC/PG/Chol bilayers, which interferes with ^{1}H decoupling and ^{1}H−^{13}C cross-polarization, but is largely immobilized in the VM+ membrane. While the two membranes both contain POPC and cholesterol, POPE and sphingomyelin have significantly higher phase transition temperatures than POPG; thus, the VM+ membrane is more viscous than the PC/PG/Chol membrane, slowing down BM2(1−33) motion.

DNP experiments at cryogenic temperature (~117 K) enhanced the sensitivity sufficiently to allow us to resolve the BM2 signals from the lipid background signals through ^{15}N−^{13}C and ^{13}C−^{13}C dipolar filters (Figure 2c−e). A sensitivity enhancement factor of 21−27 was achieved using a recently optimized membrane preparation protocol for DNP NMR.[41]

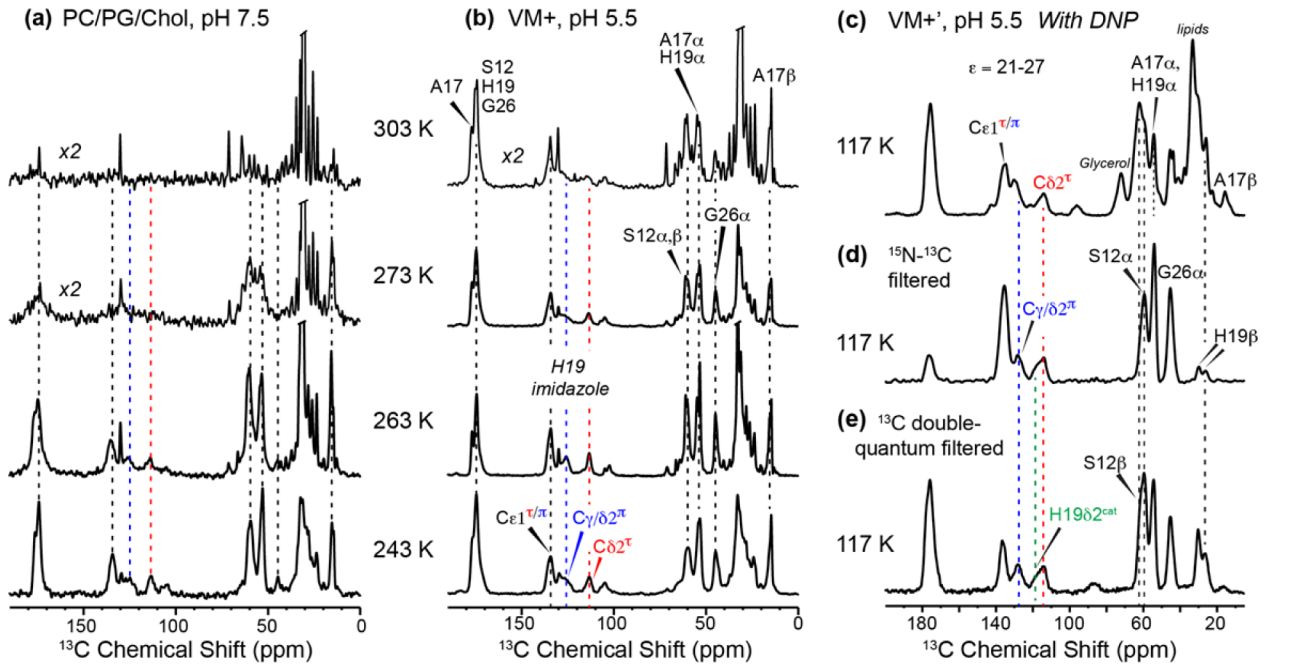

Figure 2. One-dimensional ^{13}C CP-MAS spectra of BM2(1−33) as a function of pH, temperature, and membrane composition. (a) BM2 in the PC/PG/Chol membrane at pH 7.5. (b) BM2 in the VM+ membrane at pH 5.5. The VM+ membrane immobilizes the peptide while the PC/PG/Chol membrane promotes peptide motion at high temperature. (c−e) DNP-enhanced ^{13}C spectra of BM2 at pH 5.5 in a partially deuterated VM+ membrane. (c) ^{13}C CP spectrum with MW on. The sensitivity is 21−27 times that of the MW-off spectrum (not shown). (d) ^{15}N−^{13}C dipolar filtered ^{13}C spectrum. (e) ^{13}C DQF spectrum.

DOI: 10.1021/jacs.6b03142
J. Am. Chem. Soc. 2016, 138, 8143−8155

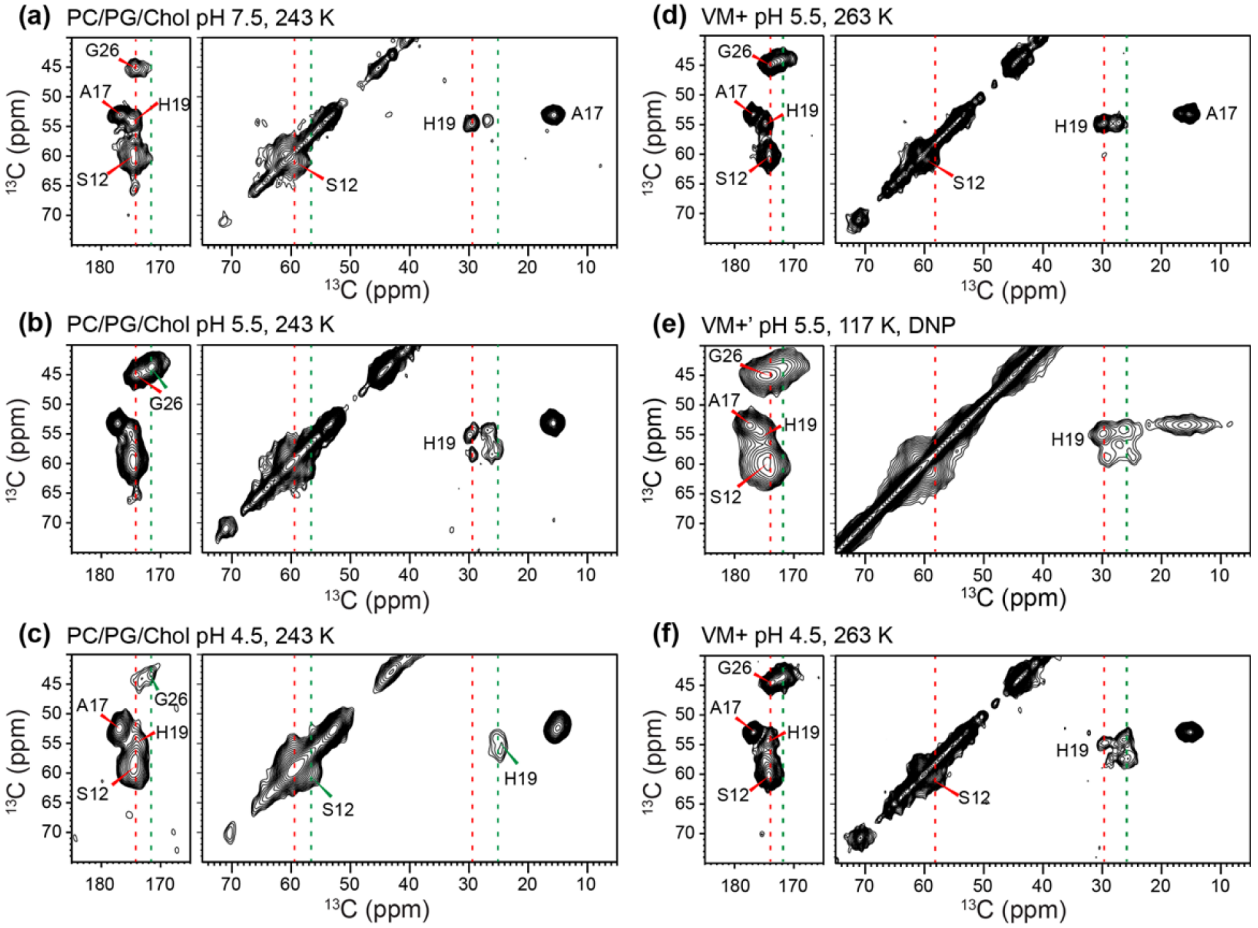

Figure 3. Two-dimensional $^{13}C-^{13}C$ correlation spectra of site-specifically labeled BM2(1−33) in different membranes and at different pH. (a) PC/PG/Chol at pH 7.5. (b) PC/PG/Chol at pH 5.5. (c) PC/PG/Chol at pH 4.5. (d) VM+ membrane at pH 5.5. (e) VM+′ membrane at pH 5.5 with DNP. (f) VM+ membrane at pH 4.5.

Table 1. ^{13}C and ^{15}N Chemicals Shifts (ppm) of BM2(1−33)[a]

residue	N	CO	Cα	Cβ	Cγ	Cδ2	Cε1	Nδ1	Nε2
S12, pH 7.5	119.1	174.6	59.4	60.9					
S12, pH 4.5	118.0	174.5	57.9	59.8					
A17, pH 7.5	123.8	176.7	53.1	15.7					
A17, pH 4.5	125.2	177.0	52.4	15.0					
H19, τ	118.9	174.7	54.8	29.7	135.6	113.6	134.3	250.9	162.6
H19, π	119.0	174.6	54.3	27.1	125.9	124.5	134.6	171.0	251.2
H19, cat1	118.8	174.4	58.0	28.9	134.4	116.4	135.9	-	171.1
H19, cat2	118.5	174.4	54.3	26.1	128.0	116.0	134.3	177.2	175.2
H19, cat3	118.5	174.4	57.2	25.3	126.4	117.3	133.2	175.7	174.8
G26, pH 7.5	106.2	174.1	45.2						
G26, pH 4.5	105.6	171.5	43.4						

[a]The chemical shifts of S12, A17, and G26 are obtained from the PC/PG/Chol sample data, while the H19 chemical shifts are average values of the PC/PG/Chol and VM+ data. All ^{13}C chemical shifts were taken from 2D $^{13}C-^{13}C$ correlation experiments at low temperature, while ^{15}N chemical shifts were taken from 1D ^{15}N and 2D $^{15}N-^{13}C$ correlation spectra at low temperature.

With the removal of the natural abundance ^{13}C signals of lipids and cryoprotectants, we resolved two His19 Cβ signals at 29 and 27 ppm and the S12 Cα and Cβ signals at ∼60 ppm (Figure 2d,e).

pH- and Membrane-Dependent Structures of His19. One-dimensional ^{13}C spectra (Figure 2), 2D $^{13}C-^{13}C$ correlation spectra (Figure 4), and 2D $^{15}N-^{13}C$ correlation spectra (Figure 5) provide detailed information on the chemical structure of the proton-selective residue, His19, under different pH and membrane compositions. In the aromatic region of the 1D spectra (Figure 2), both the pH 7.5 PC/PG/Chol sample and the pH 5.5 VM+ sample show Cγ and Cδ2 chemical shifts of ∼135 ppm and ∼114 ppm, which are diagnostic of neutral histidines. The DNP-enhanced spectra show additional intensities at ∼118 ppm, which can be assigned to Cδ2 of cationic histidine. Two-dimensional $^{13}C-^{13}C$ correlation spectra (Figure 4) allowed unambiguous assignment of the ^{13}C signals of the various tautomeric and cationic states of histidine. In the aliphatic region, the pH 7.5 PC/PG/Chol sample and the pH 5.5 VM+ sample both

DOI: 10.1021/jacs.6b03142
J. Am. Chem. Soc. 2016, 138, 8143−8155

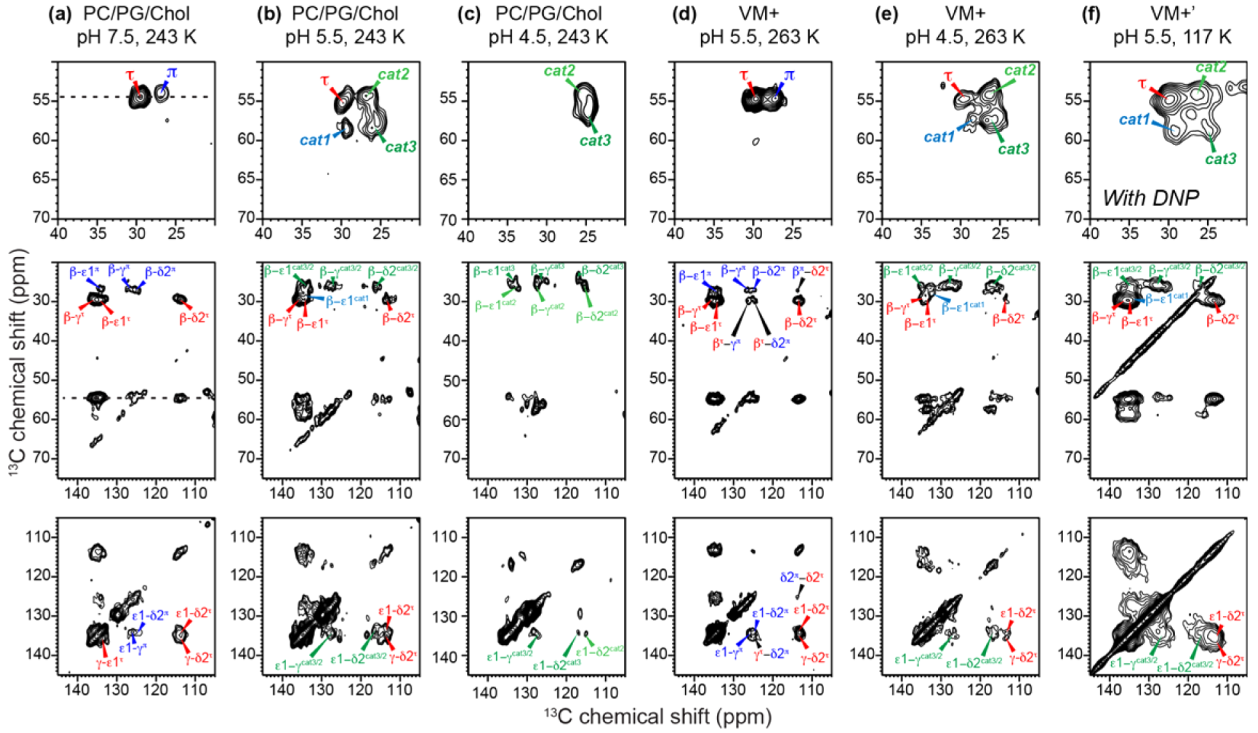

Figure 4. His19 regions of the 2D ^{13}C−^{13}C correlation spectra of BM2(1−33) at different pH and in different lipid membranes. The spectra in parts a−c were measured at 243 K on PC/PG/Chol bound peptide. (a) pH 7.5, (b) pH 5.5, (c) pH 4.5. The spectra in parts d−e were measured at 263 K on VM+ bound peptide at (d) pH 5.5 and (e) pH 4.5. (f) DNP-enhanced spectrum of BM2(1−33) in the d_{31}-VM+′ membrane at pH 5.5. Spectra a−c were measured on a 400 MHz spectrometer under 7 kHz MAS, while spectra d−e were measured on an 800 MHz spectrometer with 14.5 kHz MAS. The DNP spectrum (f) was measured on a 400 MHz/263 GHz spectrometer at 117 K under 9 kHz MAS. The DARR mixing times were 50 or 100 ms in these spectra.

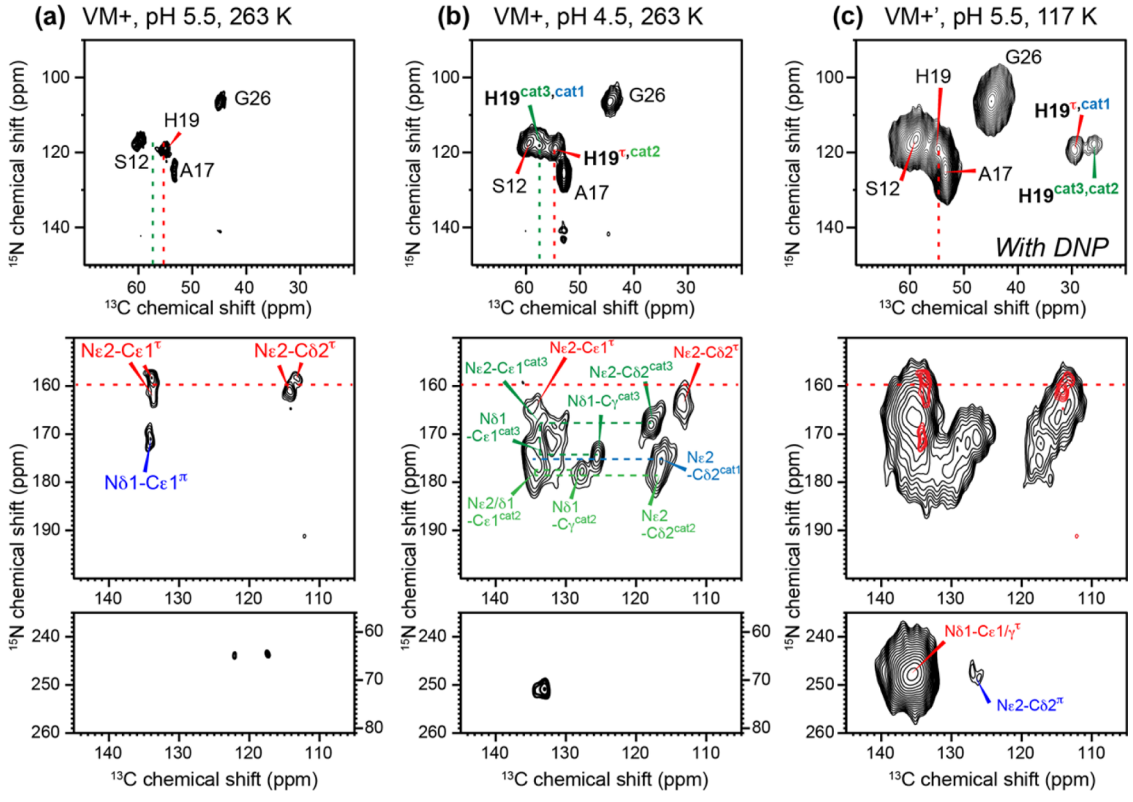

Figure 5. Two-dimensional ^{15}N−^{13}C correlation spectra of His19 in BM2(1−33). (a, b) BM2 in the VM+ membrane, measured on an 800 MHz spectrometer with 14.5 kHz MAS at 263 K. (a) pH 5.5, (b) pH 4.5, (c) BM2 at pH 5.5 in the d_{31}-VM+′ membrane, measured on a 400 MHz/263 GHz DNP spectrometer under 9 kHz MAS at 117 K. Note the different neutral and cationic histidine distribution between high and low temperatures at pH 5.5, indicating temperature-induced pK_a shifts.

DOI: 10.1021/jacs.6b03142
J. Am. Chem. Soc. 2016, 138, 8143−8155

show two Cα-Cβ cross peaks, while the pH 5.5 PC/PG/Chol sample and the pH 4.5 VM+ sample exhibit four Cα-Cβ peaks. The nature of these Cα-Cβ peaks can be identified on the basis of their correlations with the side chain Cε1, Cδ2, and Cγ chemical shifts.[19,22,51] For the higher-pH spectra, the (54.8, 29.7) ppm cross peak can be assigned to the τ tautomer due to its correlation with the 113.5 ppm chemical shift of Cδ2, while the (54.3, 27.1) ppm cross peak can be assigned to the π tautomer because of its connectivity to the 124 ppm Cδ2 peak. In the lower-pH spectra, the τ tautomer Cα-Cβ peak is still present, while two cross peaks with Cβ chemical shifts of ∼26 ppm can be assigned to cationic histidines, cat2 and cat3, on the basis of their correlations with Cγ and Cδ2 chemical shifts of ∼127 and ∼117 ppm. The fourth cross peak at (58.0, 28.9) ppm is correlated with the same Cε1 and Cγ peaks as the τ tautomer, but also correlates with a 116.5-ppm Cδ2 peak, which thus reveals it to be a cationic histidine. This state is similar to the previously observed cat1 state of AM2 His37.[20] Finally, in the pH 4.5 PC/PG/Chol sample, the spectrum simplifies to only cationic histidine, with two partially overlapped Cα-Cβ cross peaks (Figure 4c). These chemical shifts are summarized in Table 1.

These 2D $^{13}C-^{13}C$ correlation spectra show that the VM+ membrane produces the same set of His19 structures as the PC/PG/Chol membrane, but at 1−2 lower pH units. Thus, the negatively charged membrane facilitates proton association with His19. The τ and π tautomers that coexist in the pH 5.5 VM+ membrane have weak but clear cross peaks with each other, for example, between the τ Cβ chemical shift and the π Cγ chemical shift at (30, 126) ppm and between π Cδ2 and τ Cδ2 at (125, 114) ppm (Figure 4d). These intertautomer cross peaks indicate that both τ and π tautomers exist in the same tetramer instead of being separated into different channels.[23]

Two-dimensional $^{15}N-^{13}C$ HETCOR spectra (Figure 5) give complementary information about the pH-dependent structure distribution of His19. At pH 5.5, the backbone N−Cα cross peaks show relatively narrow linewidths of 1.5 ppm. Decreasing the pH to 4.5 increased the backbone linewidths, similar to the situation of the 2D $^{13}C-^{13}C$ correlation spectra. The aromatic region of the 2D spectrum is simple for the pH 5.5 sample, with two τ tautomer peaks and one π tautomer peak (Figure 5a). But at pH 4.5 the 2D spectrum is much more complex, showing multiple cationic species (Figure 5b). Four Nε2-Cδ2 cross peaks are resolved at ^{13}C chemical shifts of 113−118 ppm, and can be assigned to the τ tautomer and three cationic histidines, while two Nδ1-Cγ cross peaks are observed and can be assigned to cat2 and cat3.

Figure 6 compares the pH-dependent 2D $^{13}C-^{13}C$ correlation spectra encoding the ^{13}C chemical shifts of His19 in BM2 and His37 in AM2. With decreasing pH, His19 progresses from a dual τ−π tautomeric mixture to a four-state neutral and cationic mixture. This change occurs from pH 7.5 to pH 5.5 in the PC/PG/Chol membrane and from pH 5.5 to pH 4.5 in the VM+ membrane. At sufficiently low pH, which is 4.5 for the PC/PG/Chol membrane and pH 4.0 for the VM+ membrane, a single cationic state is observed. The cytoplasmic-containing

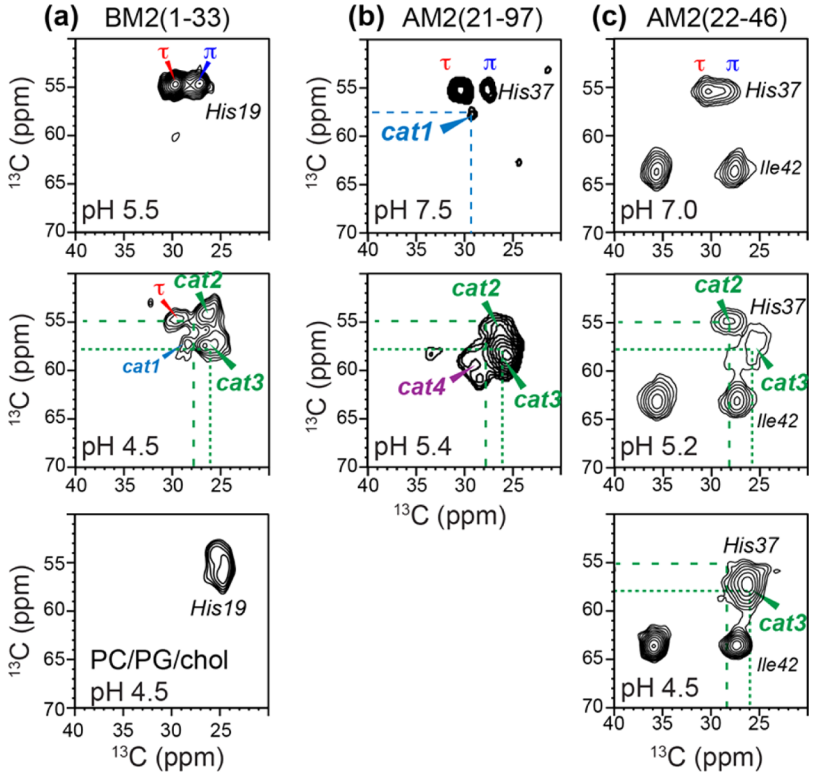

Figure 6. Comparison of His19 and His37 conformational distribution in BM2 and AM2 from 2D $^{13}C-^{13}C$ correlation spectra. All peptides and proteins were bound to eukaryotic-mimetic lipid membranes, except for the pH 4.5 spectrum of BM2, which was bound to the PC/PG/Chol membrane. Spectra were measured at moderate low temperatures (243−273 K) where the peptides and proteins are immobilized. (a) BM2(1−33) in VM+ membranes at pH 5.5 and pH 4.5, and BM2(1−33) in the PC/PG/Chol membrane at pH 4.5. (b) AM2(21−97) in the VM+ membrane at pH 7.5 and pH 5.4. (c) AM2 TM peptide (residues 22−46) in the VM membrane at pH 7.0, 5.2, and 4.5. BM2 His19 exhibits the largest number of coexisting species, at pH 4.5. The fact that neutral tautomers persist to lower pH in BM2 indicates that His19 protonates with lower and more clustered pK_a's. The spectrum of the pH 4.5 VM+ bound BM2 resembles the spectrum of the PC/PG/Chol bound BM2 at pH 5.5 in Figure 4b, indicating the influence of the negatively charged lipid on the protonation equilibria.

DOI: 10.1021/jacs.6b03142
J. Am. Chem. Soc. 2016, 138, 8143−8155

AM2(21−97) also resolved four cationic His37 species, cat1 to cat4 (Figure 6b), with similar chemical shifts as those of BM2 His19; however, the four states do not occur at the same pH. These four species have been assigned to histidines in variously charged tetrads, +1 to +4, based on the pH at which they become populated.[20] The shorter AM2 TM peptide also showed similar tautomeric chemical shifts (Figure 6c), but fewer cationic species were found compared to the cytoplasmic-containing AM2. Importantly, the pH at which the multiple histidine states appear differs qualitatively between BM2 and AM2: BM2 concentrates a larger number of histidine species into a narrower pH range, which is around pH 4.5 for the VM+ membrane and about pH 5.5 for the PC/PG/Chol membrane. AM2(21−97) shows three cationic species at pH 5.4 while AM2(22−46) shows only two cationic states at pH 5.2. Since these AM2 and BM2 spectra were measured in similar eukaryotic-mimetic lipid mixtures of VM+ and VM, the different pH dependences reflect real differences in the acid-dissociation equilibria of the histidines. Specifically, BM2 His19 retains neutral tautomers to lower pH than His37 in AM2, indicating lower pK_a's (*vide infra*).

DNP-Enhanced 2D Spectra at Cryogenic Temperature. Sensitivity enhancement by DNP allowed the observation of additional features in 2D $^{13}C-^{13}C$ and $^{15}N-^{13}C$ correlation spectra at pH 5.5 (Figures 4f and 5c). Where previously only neutral τ and π tautomers were detected at 263 K, we now also observe the signals of cat1, cat2, and cat3, while the π tautomer cross peaks are below the detection limit (Figure 4f). Spectral integration indicates that the cationic species represent 50−60% of the total intensities under the DNP experimental condition, while the higher-temperature 2D spectra at pH 5.5 do not show detectable cationic histidine intensities. Instead, the DNP spectrum at pH 5.5 is more similar to the high-temperature 2D spectrum at pH 4.5, which shows ~80% cationic intensities. This suggests that the effective pK_a's of the histidine are higher at cryogenic temperature than at high temperature. The 2D $^{15}N-^{13}C$ correlation spectrum (Figure 5c) shows similar results, with the intensity pattern approaching the pH 4.5 spectrum at high temperature (Figure 5b).

His19 Proton Exchange Equilibria and Dynamics. To obtain quantitative information about the His19 protonation equilibria, we measured the 1D ^{15}N CP-MAS spectra of VM+ bound BM2 from pH 6.5 to pH 4.0. Since there are in principle four acid-dissociation constants for the tetrameric channel, the pK_a extraction requires a minimum of four samples. The spectra were measured at 243 K where proton-transfer dynamics are suppressed. Figure 7a shows the expected progressive decrease of the 250 ppm unprotonated ^{15}N peak intensity with decreasing pH. As shown before,[19] the relative concentration of neutral and cationic histidines can be obtained from the intensity ratio I_{NH}/I_N. Figure 8b and Table 2 show that [His]/[HisH$^+$] decreases rapidly from 10.8 to 0.14 over the pH range 6.5−4.0 for the VM+ bound peptide. Fitting these values to eq 1 yielded pK_a's of 6.1 ± 0.1, 5.7 ± 0.1, 4.5 ± 0.3, and 4.2 ± 0.4. The two lowest pK_a's have the largest uncertainty, due to the fact that the unprotonated ^{15}N peak intensity is weak at pH 4.0; thus, the percentage of neutral histidines is difficult to determine with high precision. Alternative fits assuming only two distinct pK_a's can also agree with the data, and extraordinarily high precision and accuracy in the concentration ratios as well as the sample pH would be required to distinguish these different models. Nevertheless, the BM2 data differs from the recent studies of His37 in AM2(18−60) and in the cytoplasmic-containing AM2(21−97), whose ^{15}N spectra could not be adequately fit to four pK_a's.[20,53]

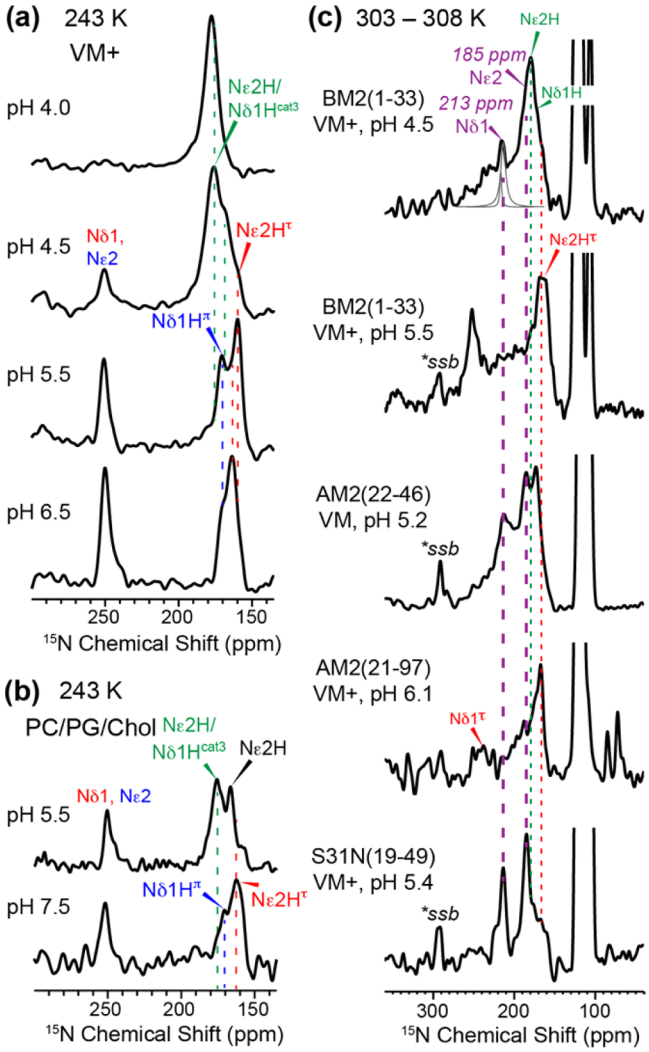

Figure 7. One-dimensional ^{15}N CP spectra of BM2(1−33) as a function of pH, membrane composition and temperature. (a) Spectra of the VM + bound BM2 from pH 4.0 to pH 6.5 at 243 K. (b) Spectra of PC/PG/Chol-bound BM2 at pH 5.5 and pH 7.5 at 243 K. (c) Comparison of high-temperature (303−308 K) ^{15}N spectra of BM2 and AM2 at acidic pH. An ^{15}N exchange peak is detected at ~213 ppm at pH 4.5 for BM2, at pH 5.2 for AM2-TM, and at pH 5.4 in the S31N mutant of AM2-TM. The exchange-averaged chemical shifts are the same in all M2 samples, but the exchange linewidths differ. The BM2 exchange peak is fit (gray line) to give a line width of 400 ± 140 Hz.

Regardless of whether there are two or four distinct pK_a's, the observation that the two highest pK_a's cluster and the two lowest pK_a's cluster is unambiguous, and this translates to charged-tetrad population curves that have a high percentage of the +2 state over a relatively wide pH range, preceded by the persistence of the fully neutral (0 charge) and +1 tetrads above pH 6, and followed by quick onsets of the +3 and +4 channels below about pH 4.5 (Figure 8c).

Incorporating BM2(1−33) into the anionic PC/PG/Chol membrane caused a shifted pH dependence of the ^{15}N spectral intensities: the pH 7.5 PC/PG/Chol spectrum resembles the pH 5.5 VM+ spectrum while the pH 5.5 PC/PG/Chol spectrum approaches the pH 4.5 VM+ spectrum (Figure 7b). This is consistent with the 2D spectra that indicate a shift of the His19 protonation equilibria to higher pH in the anionic membrane compared to the neutral membrane.

DOI: 10.1021/jacs.6b03142
J. Am. Chem. Soc. 2016, 138, 8143−8155

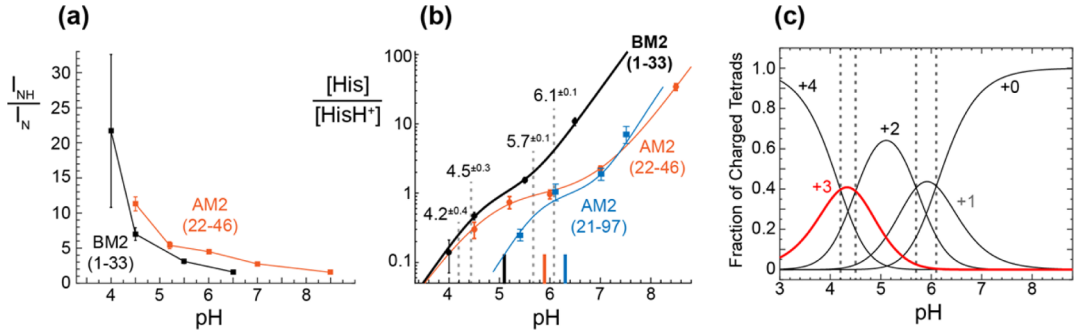

Figure 8. pK_a extraction of His19 in BM2(1−33). (a) NH to N intensity ratios as a function of pH. (b) Neutral-to-cationic histidine concentration ratios as a function of pH. The BM2 data (black) are compared with previously measured AM2 TM peptide data[54] (orange) and AM2(21−97) data (blue). The neutral histidine concentration in BM2 is higher than that of AM2 at similar pH. The extracted pK_a's for BM2 are 6.1, 5.7, 4.5, and 4.2, whose average is lower than that of AM2 constructs. The average pK_a's of the three M2 samples are indicated as solid lines at the bottom. (c) Populations of charged tetrads of His19 in BM2 as a function of pH. The intercepts of adjacent population curves correspond to the pK_a's.

Table 2. BM2(1−33) His19 Imidazole ^{15}N Intensities and Neutral to Cationic Histidine Concentration Ratios

pH	I_{NH}/I_N	κ	[His]/[HisH$^+$]
4.0	21.7 ± 10.9	1.44 ± 0.04	0.14 ± 0.07
4.5	7.0 ± 0.9	1.33 ± 0.04	0.47 ± 0.06
5.5	3.1 ± 0.3	1.35 ± 0.03	1.54 ± 0.15
6.5	1.6 ± 0.2	1.35 ± 0.04	10.8 ± 1.4

To investigate the proton-transfer kinetics, we measured ^{15}N CP spectra at high temperature (Figure 7c). Since BM2 tetramers undergo intermediate-time scale motion in the PC/PG/Chol membrane, high-temperature intensities can only be observed for VM+ bound peptide. At 303−308 K, the pH 5.5 VM+ sample retained the neutral tautomer peaks at 251 ppm and 160−170 ppm, but in addition a broad band of intensities between 170 and 250 ppm emerged, suggesting chemical exchange of the imidazole nitrogens with a distribution of equilibrium constants. Most importantly, at pH 4.5, the spectrum exhibits an exchange peak at 213 ppm and additional intensities at ∼185 ppm. These intermediate ^{15}N chemical shifts are identical to the values seen for His37 in AM2, and can be assigned to Nε2 and Nδ1 chemical exchange among the τ tautomer, π tautomer, and cationic histidine.[19,22] Thus, the chemical-exchange equilibria among the three histidine states are conserved between AM2 and BM2.

BM2 Channel Hydration from Water−Protein 2D Correlation Experiments. To investigate whether BM2 channel hydration differs from that of AM2, we measured 2D water−peptide ^{1}H−^{13}C correlation spectra as a function of the ^{1}H spin-diffusion mixing time. Figure 9a shows a representative 2D spectrum of BM2(1−33) in the PC/PG/Chol membrane at pH 7.5, measured with a ^{1}H mixing time of 50 ms. Spectra measured at a shorter mixing time of 4 ms give information about the initial spin-diffusion rate from water to the peptide. At pH 7.5 (Figure 9b), the intensity of the short-mixing spectrum is 20−30% of the long-mixing spectrum for the Cα and Cβ peaks, while the His19 aromatic signals have higher intensities of >40%. At acidic pH, the 4 ms Cα and Cβ peak intensities increase compared to those for the higher pH sample, indicating faster water−protein polarization transfer. The His19 side chain intensities are the highest, showing 80−90% of the equilibrium intensities. Thus, BM2 is much more hydrated at low pH than at high pH, consistent with an open channel.

Figure 9e,f summarizes the S/S_0 ratios of the resolved ^{13}C signals of BM2(1−33). For each membrane, the water cross peaks are higher at low pH than at high pH. Between the two lipid membranes, the PC/PG/Chol bound BM2 exhibits higher water cross peaks than the VM+ bound peptide at the same pH, indicating that the anionic membrane facilitates channel hydration. Thus, the viscous and neutral VM+ membrane contains less hydrated BM2 channels than the PC/PG/Chol membrane. Among the four labeled residues, the His19 side chain has the highest water cross peaks, consistent with the polar and pore-facing nature of this residue. Interestingly, S12 exhibits a large pH-dependent change in the water cross-peak intensity. In the PC/PG/Chol membrane, the S/S_0 values changed from 0.29 ± 0.04 at pH 7.5 to 0.42 ± 0.04 at pH 5.5. Decreasing the pH by 1 unit in the VM+ membrane causes the S/S_0 values to increase from 0.14 ± 0.03 to 0.38 ± 0.03. The latter change is larger than that of all other residues measured so far in AM2 and BM2, including S31 in AM2 (Figure 9h), indicating that the pore-facing serine residues in BM2 play a prominent role in channel hydration, which should promote H$^+$ relay to the HxxxW motif.

DISCUSSION

The data shown here give the first detailed structural and dynamical information about the proton-conducting heart of BM2 in lipid bilayers. The chemical shifts of the four labeled residues indicate that the BM2 TM peptide is α-helical in a range of pH and in two different membranes. Although the number of labeled residues is too small to permit more detailed structural conclusions, it is nevertheless interesting that the three non-histidine residues change their chemical shifts at low pH in a direction that corresponds to less ideal α-helical conformations. This trend is opposite that of the AM2 TM peptide, which exhibits more ideal α-helical chemical shifts, and straight helices, at acidic pH.[55] The nonideal helical chemical shifts seen in BM2 may be related to the coiled coil structure found for DHPC-bound BM2, even though the solution NMR structure was solved at pH 7.5.[12] More complete structural measurements are required to elucidate the high-resolution backbone conformation and oligomeric assembly of BM2 in lipid bilayers.

The pH-dependent ^{15}N spectra and 2D correlation spectra indicate that His19 protonates at significantly lower pH than His37 in both the TM and cytoplasmic-containing constructs of AM2. The average pK_a of His19 in BM2-TM is 5.1 (Table 3). In comparison, the average pK_a's of His37 in AM2(22−46) and AM2(21−97) are 5.9 and 6.3, respectively, in similar virus-mimetic membranes.[19,20] The earliest measurement of His37 pK_a in AM2(22−46) was conducted in the significantly different

DOI: 10.1021/jacs.6b03142
J. Am. Chem. Soc. 2016, 138, 8143−8155

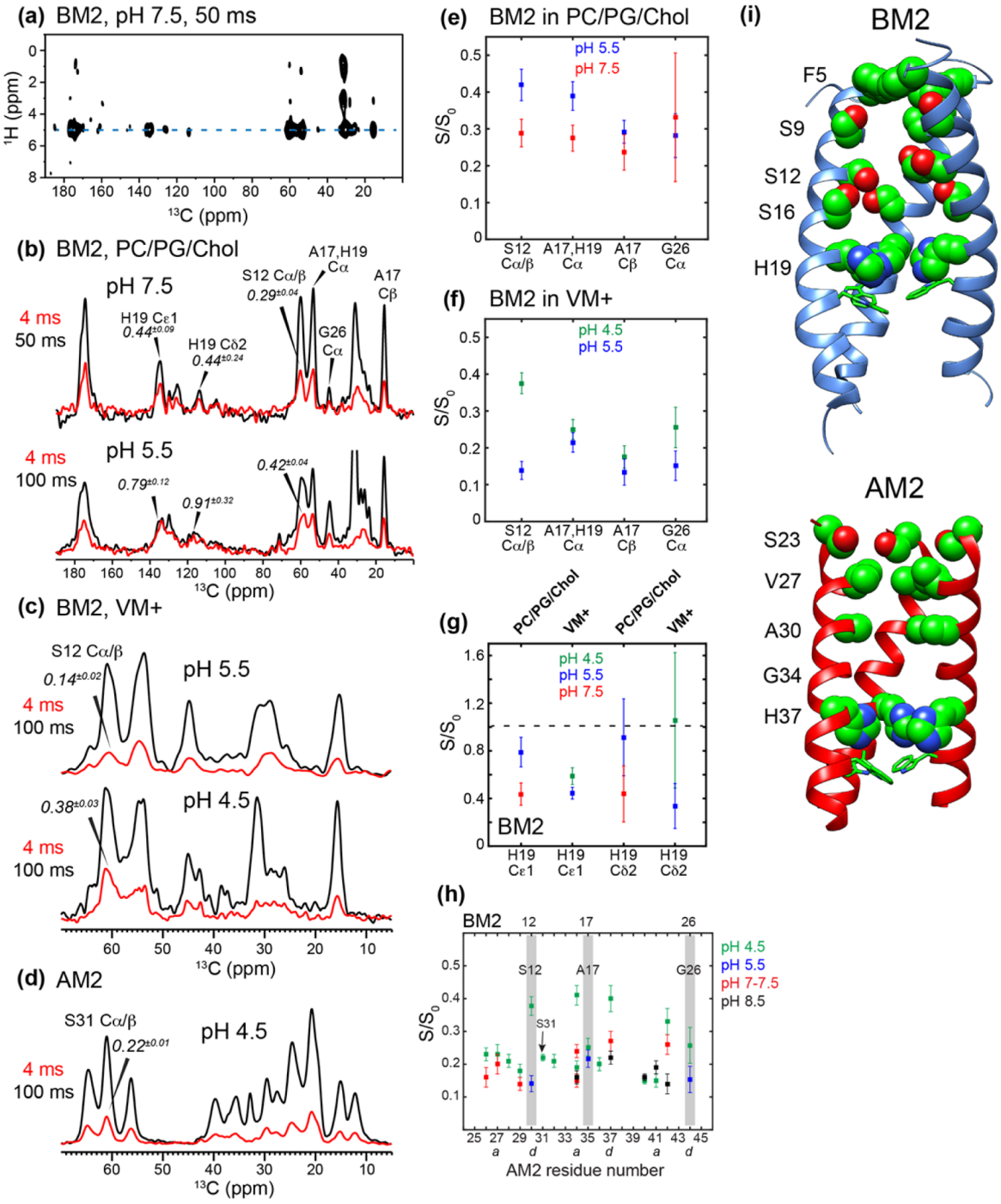

Figure 9. Two-dimensional $^{1}H-^{13}C$ HETCOR spectra of membrane-bound BM2(1−33) to probe channel hydration. (a) Representative 2D spectrum of PC/PG/Chol bound peptide at pH 7.5, measured with a ^{1}H spin-diffusion mixing time of 50 ms. (b) Water cross sections of BM2(1−33) between 4 ms and 50 or 100 ms for the pH 7.5 and pH 5.5 PC/PG/Chol samples measured at 263 K. The S/S_0 values are indicated for H19 and S12. (c) Water cross sections of the aliphatic region of the VM+ bound BM2 at pH 5.5 and pH 4.5, showing the large increase of the initial buildup of the S12-water cross-peak intensity at lower pH. (d) Water cross section of the aliphatic region of VM-bound AM2 at pH 4.5, showing that the S31 S/S_0 value is lower than that of S12 in BM2. (e) Initial buildup (S/S_0 values) at high and low pH for PC/PG/Chol-bound BM2. (f) S/S_0 values of VM+ bound BM2 at pH 5.5 and pH 4.5. (g) S/S_0 values of the His19 side chain in the two membranes. (h) S/S_0 values of the Cα sites of AM2 residues and of the BM2 residues S12, A17, and G26 (shaded bars). S12 in BM2 shows the largest low-pH induced increase of the S/S_0 value among all labeled residues of the two peptides. (i) Comparison of the solution NMR structure of BM2 (top, PDB: 2KIX) and AM2 (bottom, PDB: 2KQT) TM domains.

model membrane DMPC/DMPG, and found a much higher average pK_a of ~6.9.[24] In another recent study, the intermediate construct AM2(18−60), which includes the TM helix and the amphipathic helix, was measured in the negative-curvature membrane formed by diphytanoylphosphocholine.[56,57] This study resolved two pK_a's with an average of 6.1.[53] Therefore, despite the significant variations in the protein construct lengths and membrane compositions, the His37 pK_a's in AM2 measured under all conditions so far are higher than the BM2 His19 pK_a's found here. The His19 titration curve parallels the titration curve

DOI: 10.1021/jacs.6b03142
J. Am. Chem. Soc. 2016, 138, 8143−8155

Table 3. Comparison of Histidine pK_a's in Influenza A and B M2 Proteins in Various Lipid Membranes

M2 constructs	phospholipid membrane	His19 and His37 pK_a's	av pK_a
BM2(1−33)	POPC, POPE, SM, cholesterol	6.1, 5.7, 4.5, 4.2	5.1
AM2(22−46)[54]	DPPC, DPPE, SM, cholesterol	7.6, 6.8, 4.9, 4.2	5.9
AM2(21−97)	POPC, POPE, SM, cholesterol	7.1, 5.4	6.3
AM2(22−46)	DMPC, DMPG	8.2, 8.2, 6.3, <5.0	<6.9
AM2(18−60)	DPhPC	7.6, 4.5	6.1

of His37 in the cytoplasmic-containing AM2(21−97) but is shifted by ∼1.2 pH unit lower (Figure 8b). Compared to the AM2 TM peptide, the BM2 titration curve drops more steeply at low pH. Overall, the His19 tetrads remain predominantly in low charged states of +2, +1, and 0 until about pH 5, below which the +3 and +4 tetrad populations surge (Figure 8c). This result is found for the VM+ membrane, which is the membrane used in two of the previous four AM2 studies; thus, the pK_a decrease reflects real differences in the protonation equilibria of His19 in BM2 and His37 in AM2.

The lower pK_a's of His19 were surprising, because the BM2 channel pore is lined with polar residues such as S9, S12, and S16 (Figure 1), which would be expected to facilitate proton relay to His19 and thus stabilize the cationic state of His19. In general, altered equilibrium constants imply altered structures; thus, the BM2 TM helix structure and structural equilibrium must differ in crucial ways from the AM2 structure to account for this pK_a decrease. The solution NMR structure of micelle-bound BM2(1−33) shows a coiled coil (Figure 9i) while AM2 in the same micelles exhibits straighter helices. This secondary structure difference, if verified to persist in the lipid bilayer, may affect the proton-transfer equilibria at His19. Since there is yet no high-resolution bilayer-bound structure of BM2, we focus our consideration on the equality $K_a = k_{off}/k_{on}$ between the acid-dissociation constant and the ratio of the first-order proton-dissociation rate constant k_{off} and the second-order proton-association rate constant k_{on}. The lower pK_a's or larger K_a's indicate larger k_{off} and/or smaller k_{on}. Information about the proton-exchange kinetics is partly contained in the high-temperature His19 ^{15}N spectra (Figure 7c), which show a 213 ppm exchange peak with a full width at half-maximum of 400 ± 140 Hz. In comparison, the exchange peak of His37 in the AM2 TM peptide has a larger line width of 640 ± 70 Hz. Since proton dissociation is the rate-limiting step in proton transfer, the narrower His19 exchange peak suggests a larger k_{off} than that of His37 in AM2. Although k_{on} may be increased by the serine triplet in the N-terminal half of the TM helix, the k_{off} may increase more, thus shifting the equilibrium toward the neutral state. This interpretation of a preferentially increased k_{off} is consistent with liposome assays that indicate a larger H^+ flux of BM2(1−33) compared to AM2(18−60).[12]

What might be the structural basis for an increased proton-dissociation rate constant for His19? We propose that the second titratable histidine, His27, C-terminal to the HxxxW motif and one helical turn away from Trp23, may speed up proton release from the His19-Trp23 pair. A UV resonance Raman study showed that His27 has a higher pK_a than His19,[58] indicating that His27 is more cationic than His19 at the same pH and thus is consistent with this hypothesis. Mutation of His27 to Ala was found to decrease the H^+ conductance by ∼25% compared to the wild-type, indicating that His27 plays an active role in H^+ conduction through the BM2 channel. Importantly, this second histidine is absent in the AM2 TM domain, whose equivalent position harbors an Arg45, which is constitutively charged under the full pH range of the channel. Thus, this single amino acid difference may explain the observed destabilization of the cationic state of His19 or the lowering of the pK_a's.

At high temperature, the exchange-averaged ^{15}N chemical shifts (213 ppm and ∼185 ppm) of BM2 are the same as for AM2. We have previously shown that this interconversion among different histidine structures is most observable in low charged tetrads,[22] because they contain a high concentration of neutral histidine, and correspond a concentration ratio of 2:1:1 for the interconverting τ tautomer, π tautomer, and cationic histidine. Thus, the resolved ^{15}N chemical exchange peak does not reflect the full population distribution, and an altered histidine−water proton-transfer equilibrium at low temperature can coexist with a conserved histidine interconversion equilibrium at high temperature.

The above quantified pK_a's are obtained from BM2 bound to the neutral and relatively viscous VM+ membrane. The membrane composition also affects the relative concentrations of neutral and cationic histidines. The ^{15}N spectra of the peptide in the anionic and more fluid PC/PG/Chol membrane clearly indicate that His19 protonates at higher pH in this membrane. We attribute this change to increased local proton concentrations and enhanced protein conformational motions necessary for proton binding and release in the negatively charged and fluid PC/PG/Chol membrane. If the former accounts for the entire extent of change in the cationic/neutral histidine concentration ratios, then the true equilibrium constant would be unaffected because the higher local H^+ density rather than the average sample pH should be used in considering the equilibrium constant. The importance of electrostatic charges on the H^+ transfer equilibria is also observed in a recent study of the cytoplasmic-containing AM2, which shows higher pK_a's for His37 than the TM peptide. This result was attributed to the anionic nature of the cytoplasmic domain,[20] which should elevate the local proton concentrations.

The NMR observed reduction of BM2 His19 pK_a's compared to AM2 His37 differs from UV resonance Raman data, which found that AM2 His37 has an average pK_a of 5.7[27] while BM2(3−33) exhibits a midpoint of transition at pH ∼ 6.5 for the pH-dependent quenching of W23 fluorescence emission by His19.[58] These resonance Raman data were obtained from POPE/POPS (1:1) bound peptides. Two possible reasons could explain this discrepancy. First, the negatively charged POPE/POPS membrane may affect the BM2 and AM2 protonation equilibria differently in comparison to the neutral VM+ membranes used in the solid-state NMR experiments. Second, fluorescence quenching can be caused by changes in the environmental polarity and mobility of the Trp side chain, in addition to the His-Trp cation−π interaction; thus, the interpretation of the resonance Raman spectra has inherent uncertainty. In comparison, the ^{15}N NMR chemical shifts are unambiguous indicators of the chemical structure of histidine.

The water−peptide 2D correlation spectra show increased hydration at low pH than at high pH for BM2, similar to the AM2 behavior.[46] The negatively charged PC/PG/Chol membrane at pH 7.5 gives higher water cross peaks than the VM+ membrane at pH 5.5, indicating that the VM+ membrane causes a tighter and less hydrated channel. The increased pore hydration at more acidic pH should facilitate His19 protonation by delivering

DOI: 10.1021/jacs.6b03142
J. Am. Chem. Soc. 2016, 138, 8143−8155

protons through the water molecules rapidly to histidine. Interestingly, the VM+ bound S12 exhibits the largest pH-dependent increase of the water cross-peak intensity among all residues measured so far in both BM2 and AM2. This acid-induced hydration increase is not solely due to the pH dependence of chemical exchange between the serine hydroxyl group and water, because S31 in AM2 does not show a particularly high S/S_0 value at low pH, and S12 at pH 5.5 has similar water cross-peak intensities as the nonexchangeable A17 and G26. It is known that the chemical exchange rate of serine OH is ~900 s^{-1} at pH 7 and 35 °C, which is 2-fold smaller than the proton exchange rate of imidazole NH (1700 s^{-1}).[59] Yet, here S12 Cα has higher S/S_0 than H19 Cα at pH 4.5 (Figure 9f). Thus, S12 hydration is truly increased at low pH, suggesting that this residue is important for mediating proton relay to the HxxxW motif.

The DNP spectra at cryogenic temperature show moderate differences in the pH equilibria of His19 from the high-temperature data. For the pH 5.5 sample, the concentration of cationic histidine increased to 40−50%, while at 263 K mainly neutral histidines are observed at the same prepared pH. We attribute this increased cationic concentration at low temperature to the different temperature dependences of the buffer and the imidazole pK_a's. The citrate buffer pK_a has a linearly extracted temperature coefficient $d(pK_a)/dT$ of −0.01,[60,61] while the imidazole pK_a has a larger temperature coefficient of −0.02. Thus, as the sample temperature decreases, the citrate pK_a should increase but to a smaller extent than the imidazole pK_a. This means that, at low temperature, the imidazole side chain will be more readily protonated by the buffer. The thermodynamic parameters for the ionization of buffer ions and imidazoles are not known to very low temperatures, and the exact freezing temperature of the channel water is also unknown. However, the relative trend that the imidazole pK_a has a more negative temperature coefficient than the citrate pK_a's is reliable, and favors protonation of His19 at low temperature. A potential acid−base equilibrium change between cryogenic temperature and ambient temperatures should thus be taken into account in DNP NMR experiments of pH-sensitive proteins and other biomolecules in buffered solution.

CONCLUSIONS

In its global conformational and dynamical behavior, BM2(1−33) is similar to the AM2 TM peptide: the tetrameric channel is α-helical and undergoes intermediate-time scale motion in low-viscosity membranes at physiological temperature. However, important differences are found at the proton-selective histidine in the HxxxW motif, and in the pore-lining residues leading to this motif. His19 in BM2 remains neutral down to lower pH than His37 AM2, and cationic His19 appears in a narrower pH range than His37 in AM2. Thus, His19 in the tetrameric BM2 channel protonates with lower and more clustered pK_a's. Quantitative analysis of the ^{15}N spectra yielded pK_a values of 6.1, 5.7, 4.5, and 4.2, which are about 1 pH unit lower than His37 in AM2. We propose that the altered pK_a's result from the presence of a second titratable histidine, C-terminal to His19, in BM2. This second histidine is absent in AM2 and likely increases the proton-dissociation rate constant of His19. This model is consistent with the narrower His19 chemical exchange peak compared to AM2 His37 and with H^+ flux and mutagenesis data. Similar to AM2, BM2 channels are more hydrated at acidic pH than at high pH, but compared to AM2, S12 in BM2 exhibits the largest acid-induced increase in the water cross-peak intensity, consistent with the model that the Ser triplet lining the BM2 pore facilitates proton relay to His19 by increasing pore hydration. We found that the lipid membrane also plays a significant role in proton-transfer dynamics and channel hydration: anionic membranes facilitate His19 protonation at high pH and increase the channel hydration compared to neutral membranes. These results give rich insights into how the amino acid sequence and the membrane environment affect the functional structure and dynamics of this family of viral proton channels.

AUTHOR INFORMATION

Corresponding Author

*meihong@mit.edu

Present Address

§Eduard-Zintl-Institute of Inorganic and Physical Chemistry, Technische Universität Darmstadt, Alarich-Weiss-Straße 8, 64287 Darmstadt, Germany.

Notes

The authors declare no competing financial interest.

ACKNOWLEDGMENTS

This work is supported by NIH Grant GM088204 to M.H. The authors would like to thank Dr. Ivan Sergeyev (Bruker Biospin) for help with measuring the DNP NMR spectra.

REFERENCES

(1) Brammer, L.; Kniss, K.; Epperson, S.; Blanton, L.; Mustaquim, D.; Steffens, C.; D'Mello, T.; Perez, A.; Dhara, R.; Chaves, S. S.; Elal, A. A.; Gubareva, L.; Wallis, T.; Xu, X.; Villanueva, J.; Bresee, J.; Cox, N.; Finelli, L.; Havers, F. *Influenza Activity—United States, 2012−13 Season and Composition of the 2013−14 Influenza Vaccine; Morbidity and Mortality Weekly Report*; Centers for Disease Control and Prevention, Atlanta, 2013.

(2) Koutsakos, M.; Nguyen, T.; Barclay, W.; Kedzierska, K. *Future Microbiol.* **2016**, *11*, 119.

(3) Cady, S. D.; Schmidt-Rohr, K.; Wang, J.; Soto, C. S.; DeGrado, W. F.; Hong, M. *Nature* **2010**, *463*, 689.

(4) Cady, S. D.; Hong, M. *Proc. Natl. Acad. Sci. U. S. A.* **2008**, *105*, 1483.

(5) Stouffer, A. L.; Acharya, R.; Salom, D.; Levine, A. S.; Di Costanzo, L.; Soto, C. S.; Tereshko, V.; Nanda, V.; Stayrook, S.; DeGrado, W. F. *Nature* **2008**, *451*, 596.

(6) Pinto, L. H.; Dieckmann, G. R.; Gandhi, C. S.; Papworth, C. G.; Braman, J.; Shaughnessy, M. A.; Lear, J. D.; Lamb, R. A.; DeGrado, W. F. *Proc. Natl. Acad. Sci. U. S. A.* **1997**, *94*, 11301.

(7) Hong, M.; Fritzsching, K. J.; Williams, J. K. *J. Am. Chem. Soc.* **2012**, *134*, 14753.

(8) Mould, J. A.; Paterson, R. G.; Takeda, M.; Ohigashi, Y.; Venkataraman, P.; Lamb, R. A.; Pinto, L. H. *Dev. Cell* **2003**, *5*, 175.

(9) Pinto, L. H.; Lamb, R. A. *J. Biol. Chem.* **2006**, *281*, 8997.

(10) Tang, Y.; Zaitseva, F.; Lamb, R. A.; Pinto, L. H. *J. Biol. Chem.* **2002**, *277*, 39880.

(11) Ma, C.; Soto, C. S.; Ohigashi, Y.; Taylor, A.; Bournas, V.; Glawe, B.; Udo, M. K.; DeGrado, W. F.; Lamb, R. A.; Pinto, L. H. *J. Biol. Chem.* **2008**, *283*, 15921.

(12) Wang, J.; Pielak, R. M.; McClintock, M. A.; Chou, J. J. *Nat. Struct. Mol. Biol.* **2009**, *16*, 1267.

(13) Ma, C.; Polishchuk, A. L.; Ohigashi, Y.; Stouffer, A. L.; Schön, A.; Magavern, E.; Jing, X.; Lear, J. D.; Freire, E.; Lamb, R. A.; DeGrado, W. F.; Pinto, L. H. *Proc. Natl. Acad. Sci. U. S. A.* **2009**, *106*, 12283.

(14) Hatta, M.; Goto, H.; Kawaoka, Y. *J. Virol.* **2004**, *78*, 5576.

(15) Betakova, T.; Kollerova, E. *Acta Virologica* **2006**, *50*, 187.

(16) Betakova, T.; Hay, A. J. *Arch. Virol.* **2009**, *154*, 1619.

(17) Imai, M.; Watanabe, S.; Ninomiya, A.; Obuchi, M.; Odagiri, T. *J. Virol.* **2004**, *78*, 11007.

(18) Imai, M.; Kawasaki, K.; Odagiri, T. *J. Virol.* **2008**, *82*, 728.

DOI: 10.1021/jacs.6b03142
J. Am. Chem. Soc. 2016, 138, 8143−8155

(19) Hu, F.; Schmidt-Rohr, K.; Hong, M. *J. Am. Chem. Soc.* **2012**, *134*, 3703.
(20) Liao, S. Y.; Yang, Y.; Tietze, D.; Hong, M. *J. Am. Chem. Soc.* **2015**, *137*, 6067.
(21) Miao, Y.; Fu, R.; Zhou, H. X.; Cross, T. A. *Structure* **2015**, *23*, 2300.
(22) Williams, J. K.; Tietze, D.; Wang, J.; Wu, Y.; DeGrado, W. F.; Hong, M. *J. Am. Chem. Soc.* **2013**, *135*, 9885.
(23) Hu, F.; Luo, W.; Hong, M. *Science* **2010**, *330*, 505.
(24) Hu, J.; Fu, R.; Nishimura, K.; Zhang, L.; Zhou, H. X.; Busath, D. D.; Vijayvergiya, V.; Cross, T. A. *Proc. Natl. Acad. Sci. U. S. A.* **2006**, *103*, 6865.
(25) Williams, J. K.; Zhang, Y.; Schmidt-Rohr, K.; Hong, M. *Biophys. J.* **2013**, *104*, 1698.
(26) Nishimura, K.; Kim, S.; Zhang, L.; Cross, T. A. *Biochemistry* **2002**, *41*, 13170.
(27) Okada, A.; Miura, T.; Takeuchi, H. *Biochemistry* **2001**, *40*, 6053.
(28) Sharma, M.; Yi, M.; Dong, H.; Qin, H.; Peterson, E.; Busath, D.; Zhou, H. X.; Cross, T. A. *Science* **2010**, *330*, 509.
(29) Dong, H.; Yi, M.; Cross, T. A.; Zhou, H. X. *Chem. Sci.* **2013**, *4*, 2776.
(30) Ghosh, A.; Qiu, J.; DeGrado, W. F.; Hochstrasser, R. M. *Proc. Natl. Acad. Sci. U. S. A.* **2011**, *108*, 6115.
(31) Liang, R.; Li, H.; Swanson, J. M.; Voth, G. A. *Proc. Natl. Acad. Sci. U. S. A.* **2014**, *111*, 9396.
(32) Cross, T. A.; Sharma, M.; Yi, M.; Zhou, H. X. *Trends Biochem. Sci.* **2011**, *36*, 117.
(33) Yao, H.; Lee, M. W.; Waring, A. J.; Wong, G. C.; Hong, M. *Proc. Natl. Acad. Sci. U. S. A.* **2015**, *112*, 10926.
(34) Mani, R.; Cady, S. D.; Tang, M.; Waring, A. J.; Lehrer, R. I.; Hong, M. *Proc. Natl. Acad. Sci. U. S. A.* **2006**, *103*, 16242.
(35) Cady, S. D.; Wang, T.; Hong, M. *J. Am. Chem. Soc.* **2011**, *133*, 11572.
(36) Hong, M.; DeGrado, W. F. *Protein Sci.* **2012**, *21*, 1620.
(37) Zhou, H. X.; Cross, T. A. *Annu. Rev. Biophys.* **2013**, *42*, 361.
(38) Cady, S. D.; Wang, J.; Wu, Y.; DeGrado, W. F.; Hong, M. *J. Am. Chem. Soc.* **2011**, *133*, 4274.
(39) Rossman, J. S.; Jing, X.; Leser, G. P.; Lamb, R. A. *Cell* **2010**, *142*, 902.
(40) Gerl, M. J.; Sampaio, J. L.; Urban, S.; Kalvodova, L.; Verbavatz, J. M.; Binnington, B.; Lindemann, D.; Lingwood, C. A.; Shevchenko, A.; Schroeder, C.; Simons, K. *J. Cell Biol.* **2012**, *196*, 213.
(41) Liao, S. Y.; Lee, M.; Wang, T.; Sergeyev, I. V.; Hong, M. *J. Biomol. NMR* **2016**, *64*, 223.
(42) Takegoshi, K.; Nakamura, S.; Terao, T. *Chem. Phys. Lett.* **2001**, *344*, 631.
(43) Hong, M.; Griffin, R. G. *J. Am. Chem. Soc.* **1998**, *120*, 7113.
(44) Doherty, T.; Hong, M. *J. Magn. Reson.* **2009**, *196*, 39.
(45) Huster, D.; Yao, X.; Hong, M. *J. Am. Chem. Soc.* **2002**, *124*, 874.
(46) Williams, J. K.; Hong, M. *J. Magn. Reson.* **2014**, *247*, 118.
(47) Luo, W.; Hong, M. *J. Am. Chem. Soc.* **2010**, *132*, 2378.
(48) Hong, M.; Su, Y. *Protein Sci.* **2011**, *20*, 641.
(49) Kumashiro, K. K.; Schmidt-Rohr, K.; Murphy, O. J.; Ouellette, K. L.; Cramer, W. A.; Thompson, L. K. *J. Am. Chem. Soc.* **1998**, *120*, 5043.
(50) Hohwy, M.; Rienstra, C. M.; Jaroniec, C. P.; Griffin, R. G. *J. Chem. Phys.* **1999**, *110*, 7983.
(51) Li, S.; Hong, M. *J. Am. Chem. Soc.* **2011**, *133*, 1534.
(52) Cady, S. D.; Goodman, C.; Tatko, C.; DeGrado, W. F.; Hong, M. *J. Am. Chem. Soc.* **2007**, *129*, 5719.
(53) Colvin, M. T.; Andreas, L. B.; Chou, J. J.; Griffin, R. G. *Biochemistry* **2014**, *53*, 5987.
(54) Hu, F.; Schmidt-Rohr, K.; Hong, M. *J. Am. Chem. Soc.* **2012**, *134*, 3703.
(55) Hu, F.; Luo, W.; Cady, S. D.; Hong, M. *Biochim. Biophys. Acta, Biomembr.* **2011**, *1808*, 415.
(56) Hung, W. C.; Chen, F. Y.; Huang, H. W. *Biochim. Biophys. Acta, Biomembr.* **2000**, *1467*, 198.
(57) Tristram-Nagle, S.; Kim, D. J.; Akhunzada, N.; Kucerka, N.; Mathai, J. C.; Katsaras, J.; Zeidel, M.; Nagle, J. F. *Chem. Phys. Lipids* **2010**, *163*, 630.
(58) Otomo, K.; Toyama, A.; Miura, T.; Takeuchi, H. *J. Biochem.* **2009**, *145*, 543.
(59) Liepinsh, E.; Otting, G. *Magn. Reson. Med.* **1996**, *35*, 30.
(60) Clarke, E. C. W.; Glew, D. N. *Trans. Faraday Soc.* **1966**, *62*, 539.
(61) Goldberg, R. N.; Kishore, N.; Lennen, R. M. *J. Phys. Chem. Ref. Data* **2002**, *31*, 231.

DOI: 10.1021/jacs.6b03142
J. Am. Chem. Soc. 2016, 138, 8143−8155